Journal of Luminescence 170 (2016) 663–670

Contents lists available at ScienceDirect

Journal of Luminescence

journal homepage: www.elsevier.com/locate/jlumin

NIR luminescence from erbium doped $(100-x)SiO_2$:$xZnO$ powders obtained by soft chemical synthesis

L.J.Q. Maia [a,*], J.C.V. Santos [a], J.F. Carvalho [a], R.R. Gonçalves [b], A.C. Hernandes [c], S.J.L. Ribeiro [d]

[a] GFM, IF – UFG, Campus II, C.P. 131, CEP 74001-970 Goiânia, GO, Brazil
[b] DQ, FFCLRP – USP, Av. Bandeirantes, 3900, CEP 14040-901 Ribeirão Preto, SP, Brazil
[c] GCCMC, IFSC – USP, C.P. 369, CEP 13560-970 São Carlos, SP, Brazil
[d] Institute of Chemistry – São Paulo State University – UNESP, R. Prof. Francisco Degni 55, CEP 14800-900 Araraquara, SP, Brazil

ARTICLE INFO

Article history:
Received 30 January 2015
Received in revised form
24 August 2015
Accepted 27 August 2015
Available online 6 September 2015

Keywords:
SiO_2–ZnO system
Nanostructured materials
Er^{3+} ions
Photoluminescence
Zn_2SiO_4 phase

ABSTRACT

We present the structural and optical results of $(100-x)SiO_2$:$xZnO$ compounds with $x=0$, 20, 40, 60, 80, and 100, containing 1 mol% of Er^{3+} prepared by a simple chemical route. It was evaluated the crystallization effect on the erbium ions emission around 1533 nm due to $^4I_{13/2} \rightarrow {}^4I_{15/2}$ transition. Structural analyses using X-Ray Diffraction (XRD) and Fourier Transform Infrared Spectroscopy (FTIR) techniques showed that the prepared material present crystalline phases, the ZnO hexagonal (Zincite) and Zn_2SiO_4 rhombohedral. The relative content of crystalline phases as well the optical emissions in the infrared region are dependent on the composition and heat treatments. High-resolution transmission electron microscopy revealed average 5 nm sized Zn_2SiO_4 nanocrystals homogeneously dispersed into amorphous silica-based matrix. The Er^{3+} doped Zn_2SiO_4 crystalline phase are the most promising material to be used in optical system.

1. Introduction

Rare-earth ions when incorporated into semiconductor materials have interesting optical properties that can be used in miniaturized opto-electronic systems. Erbium ions (Er^{3+}) present special luminescent properties due to 4*f* intra-levels with emissions in the ultraviolet, visible and infrared regions [1–7]. The efficiency and line shape of the emission spectra depend on the matrix in which erbium ions are inserted. Er^{3+} line emission around 1533 nm (~0.809 eV), corresponding to the $^4I_{13/2} \rightarrow {}^4I_{15/2}$ transition, is very useful in telecommunications due to the low propagation loss in silica fibers at 1.5 μm. Miniaturized systems require a host with high rare-earth dispersion, especially for optical amplifiers. Silica has been known as an excellent material for applications in telecommunication, as waveguides and optical amplifiers, but its low rare-earth solubility ($< 1 \times 10^{18}$ ions/cm^3) is a serious drawback for the miniaturization of integrated optical systems [8]. Zinc oxide (ZnO) can play an important role in such systems because it can breakdown the silica links (Si–O–Si) favoring the incorporation of higher erbium amounts, by comparing to the pure silica, due to the formation of non-bridging oxygen (Si–O$^-$, NBO). And also, ZnO can increase the absorption cross-section at ultraviolet (UV) region favoring the energy transfer to the rare-earth ions [9]. On the other side, the wide bandgap semiconductor ZnO exhibit unique physical properties, like visible luminescent emissions under UV excitation depending on the diameter and shape of nanoparticles. Thus, ZnO nanostructures appear as a promising material for opto-electronic devices [2,10–14]. For example, amplifying planar waveguide structures in Er-doped nanocrystalline ZnO films were prepared at 800 °C with a lifetime of about 7 ms due to $^4I_{13/2}$ Er^{3+} level [15,16].

Recently, Lo et al. [17] shown that single-crystalline Er-doped ZnO nanorod present an enhancement of 1540 nm emission when grown on Ag island film with appropriate annealings. Panigrahi also obtained almost uniform quantum dots of ZnO of 2–4 nm sized encapsulated within a SiO_2 matrix, but any optical properties were investigated neither the Er^{3+} incorporation [18].

Some recent works have reported on the SiO_2–ZnO powders and films in which white-light emissions were related to oxygen vacancies under UV excitation [19–22]. Such SiO_2–ZnO materials were prepared by radio-frequency (RF) sputtering [23], magnetron sputtering [24], pulsed electron-beam deposition (PED) [2], supercritical water method, and conventional sol–gel process [25]. Here, a simple and efficient synthesis route to prepare rare-earth doped SiO_2–ZnO materials is presented. In fact, there are no reports about the synthesis and near infrared emission of the $(100-x)SiO_2$:$xZnO$ system containing Er^{3+}, according to our

* Corresponding author. Tel.: +55 62 35211122; fax: +55 62 35211014.
E-mail address: lauro@ufg.br (L.J.Q. Maia).

http://dx.doi.org/10.1016/j.jlumin.2015.08.056
0022-2313/

knowledge. However, some works report on the visible emissions of doped Zn_2SiO_4 crystalline phase, known as Willemite [26,27] and Baker et al. [28] have studied the Er^{3+} emission in the Willemite phase obtained by the vapor method.

In this work, we describe a synthesis route that uses a low cost combined sol–gel and polymeric precursor methodologies. The preparation procedure is conducted at room temperature, no atmosphere or pH control is required to prepare transparent sols and homogeneous gels, which is essential to prepare multilayered films and homogeneous powders. The chemical synthesis used allowed obtain powder compounds from the SiO_2–ZnO system, and its structural and optical properties were investigated using X-Ray Diffraction (XRD), Fourier Transform Infrared Spectroscopy (FTIR), High-Resolution Transmission Electron Microscopy (HRTEM) and Photoluminescence (PL) measurements. The optimized composition of this binary system that exhibit high infrared emission from erbium ions was determined.

2. Experimental details

2.1. Powder synthesis

The used synthesis route focused on the formation of a polymer organic/inorganic network, reducing the mobility of metals, assuring molecular level homogeneity in the matrix to prevent the precipitation or phase segregation.

Citric acid (CA, $C_6H_8O_7$, 99.5% purity from Synth) was dissolved in ethanol (EtOH, C_2H_5OH, 99.5% purity from Chemycalis) at ratio of 1.0 g to 3.0 mL, followed by the addition of zinc nitrate hexahydrate ($Zn(NO_3)_2 \cdot 6H_2O$, 98% purity from Vetec). To this solution, erbium nitrate pentahydrate ($Er(NO_3)_3 \cdot 5H_2O$, 99.9% purity from Aldrich) previously dissolved in ethanol at ratio of 1.0 g to 10.0 mL was added. Tetraethyl orthosilicate (TEOS, $(C_2H_5O)_4Si$, 98% purity from Merck) and ethylene glycol (EG, $C_2H_6O_2$, 99.5% purity from Merck) were added to the solution under vigorous stirring. The molar proportion of CA to Metals (Zn + Er + Si) was 3:1, and CA to EG was 3:2.

The citric acid reacts to form metallic citrates complexes, avoiding precipitation. Ethylene glycol was added to form polymer chains linking the metal citrates by polyesterification reactions. All synthesis occurred in open containers under constant and vigorous agitation at room temperature. After synthesis, the sols were aged for 12 h at room temperature. Using this methodology, stable sols and transparent gels were obtained.

2.2. Heat treatments

The first heat treatment was performed at 150 °C for 24 h to eliminate the solvent and adsorbed water, obtaining a homogeneous dried gel. Afterwards, the gel was submitted to heat treatment at 400 °C for 24 h to eliminate organic compounds. The materials were crushed in agate mortar and annealed at 800, 900, 1000 or 1100 °C for 2 h in air, into alumina crucibles, using a conventional furnace with heating rate of 5 °C/min.

2.3. Analytical methods

The structural features were monitored using an X-ray diffractometer from Shimadzu, model XRD-6000, operating with Cu $K\alpha$ radiation at 1.54059 Å in the θ–2θ Bragg-Brentano geometry, using scan rate of 2°/min.

The Fourier transform infrared (FTIR) spectra were collected in a BOMEM MB 100 spectrometer to evaluate the vibrational modes of the synthesized materials, and the elimination of hydroxyl groups (OH). Sample powders were dispersed in KBr and pressed to form transparent pellets, and the measurements were performed in transmission geometry with resolution of 4 cm^{-1}.

The infrared emission spectra were studied under excitation at 980 nm from a diode laser with 200 mW of power. A monochromator and an InGaAs photodiode were employed to collect the signal from 1400 nm to 1700 nm.

For the PL decay emission at 1533 nm of Er^{3+} ions, a diode laser operating at 980 nm with 200 mW of power was used as excitation source, a silica lens with focal length of 100 mm to focus the excitation in a chopper with frequency of 10 Hz from Scitec, a digital oscilloscope from Tektronix 200 MHz to analyze the emission signal detected by a InGaAs photodetector. Between the sample and the photodetector a RG1000 filter was inserted to eliminate the laser light reflection. A monochromator selected the emission at 1533 nm with a resolution of 5 nm.

High-resolution transmission electron microscopy (HRTEM) images were acquired using a JEOL microscope, JEM-2100, operating at 200 keV. Statistical histogram was obtained analyzing the HRTEM images.

3. Results and discussion

3.1. Structural properties

Fig. 1(a)–(d) shows the XRD patterns of powders with different composition annealed at 800, 900, 1000 or 1100 °C. The open circles correspond to the diffraction peaks of ZnO Hexagonal crystalline phase, named as Zincite (JCPDS Card no. 36-1451) and the solid lozenge corresponds to the diffraction peaks of Zn_2SiO_4 rhombohedral crystalline phase, named as Willemite (JCPDS Card no. 70-1235).

The powders with $x=0$ ($100SiO_2$) show no diffraction peaks and for all the samples only a broad band corresponding to an amorphous phase and centered at around 21° was observed, even for the samples calcinated at 1100 °C. For heating treatments from 800 °C to 1100 °C, the samples with $x=20$ ($80SiO_2$:20ZnO) are partially crystallized, presenting, in addition to the amorphous phase, the Willemite (♦) and an unknown phase (?). The diffraction peaks of the unknown phase increase its intensity as the heating temperatures increase, becoming well defined at 1100 °C. For $x=40$ ($60SiO_2$:40ZnO) it was observed at 800 °C and 900 °C the initial crystallization of Willemite and unknown phase, however, at 1000 °C and 1100 °C only the Willemite phase was present. Three phases were observed at 800 °C for $x=60$ ($40SiO_2$:60ZnO): the Willemite (♦), Zincite (❍) and unknown (?) phase, being the Willemite the single phase observed at higher temperatures. In the powders with $x=80$ ($20SiO_2$:80ZnO) there is a mixture of the Willemite, Zincite (major phase) and unknown phases at 800 °C. At higher temperatures the two phases Willemite and Zincite are crystallized, with about the same proportion. Finally, powders for $x=100$ (ZnO) present just the expected Zincite phase in all temperature range.

In fact, it was determined the combined ranges of compositions and temperatures for which only Willemite phase (Zn_2SiO_4) is synthesized. For $x=40$ the single Willemite phase is obtained in the temperature interval from 1000 to 1100 °C, and for $x=60$ similar results was obtained in the 900–1100 °C range. Note that, as the Zn_2SiO_4 crystalline phase has $33.3SiO_2$:66.7ZnO molar ration, the SiO_2 excess appears as amorphous phase for both $x=40$ and 60 compositions. Table 1 summarizes the results regarding on the amorphous and crystalline phases depending on the composition and heat treatment.

Fig. 2 shows the FTIR spectra of samples with different composition annealed at 900 and 1100 °C. The spectra were deconvoluted

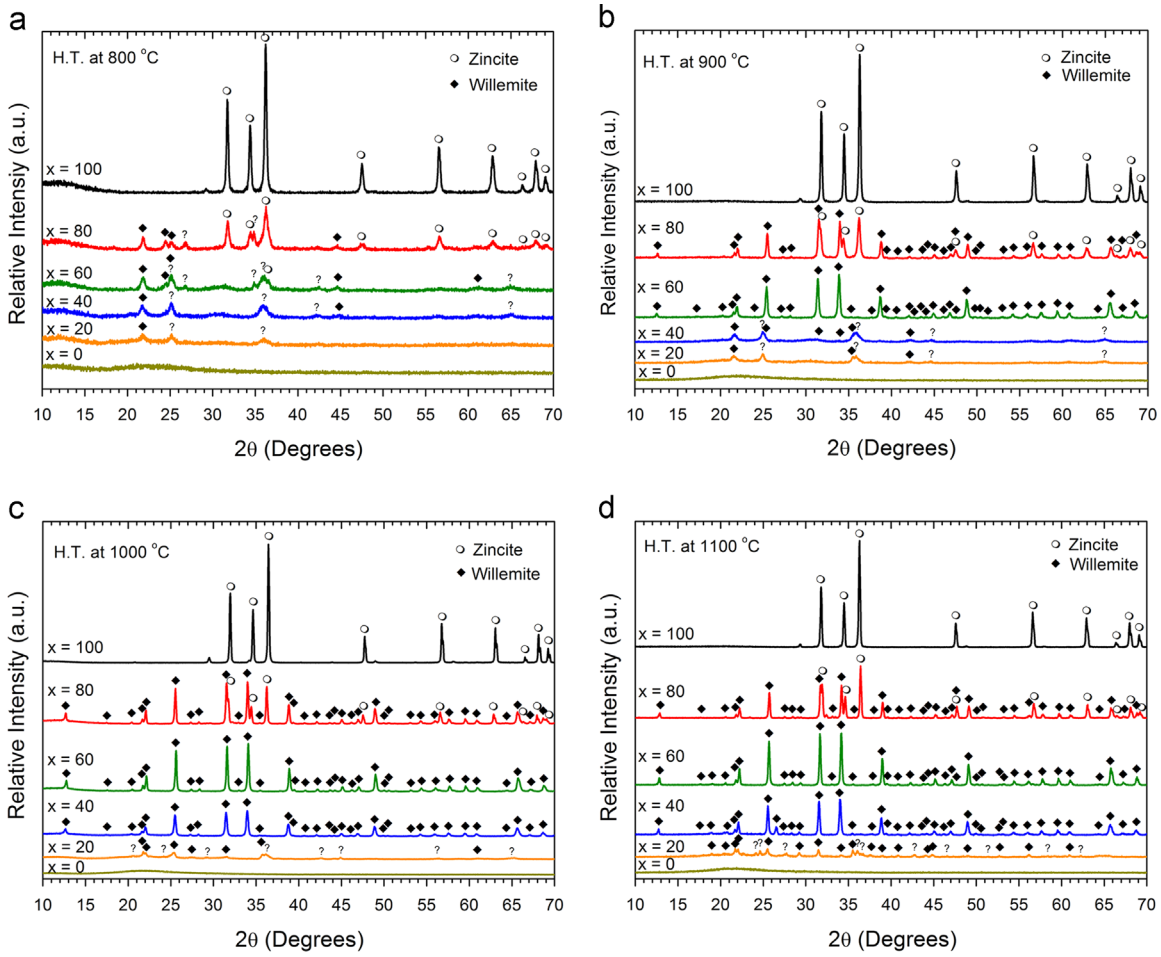

Fig. 1. X-ray diffraction patterns of $(100-x)SiO_2$:$xZnO$ powders containing 1.0 mol% of Er^{3+} annealed at (a) 800 °C, (b) 900 °C, (c) 1000 °C, and (d) 1100 °C.

Table 1
Compilation of the XRD results.

x value	Temperature (°C)			
	800	900	1000	1100
0	100% A	100% A	100% A	100% A
20	A + W + ?	A + W + ?	A + W + ?	A + W + ?
40	A + W + ?	A + W + ?	100% W	100% W
60	A + W + ? + Z	100% W	100% W	100% W
80	A + W + ? + Z	W + Z	W + Z	W + Z
100	A + Z	100% Z	100% Z	100% Z

A = Amorphous, W = Willemite, Z = Zincite, and ? = unknown phase.

in Gaussian curves and the peaks positions were listed in Table 2. The green curves are attributed to the vibrational modes of SiO_2 structure, the red ones are due to the vibration of ZnO hexagonal structure, those in blue are from Zn_2SiO_4 crystalline structure, and the orange curves are due to the unknown phase derived from silicate and zinc oxide.

As reported by Sharma and Bhatti [29] and Wu et al. [30], the Zn_2SiO_4 crystalline phase shows vibrational modes at 396 cm^{-1} (ν_4-SiO_4), 460 cm^{-1} (ν_4-SiO_4), 578 cm^{-1} (ν_1-ZnO_4), 616 cm^{-1} (ν_3-ZnO_4), 870 cm^{-1} (ν_1-SiO_4), 900 cm^{-1} (ν_3-SiO_4), 934 cm^{-1} (ν_3-SiO_4), 978 cm^{-1} (ν_3-SiO_4), 1080 cm^{-1} (ν_3-Si–O–Si), where 'ν_1' is the symmetric stretching, 'ν_3' is the asymmetric stretching and

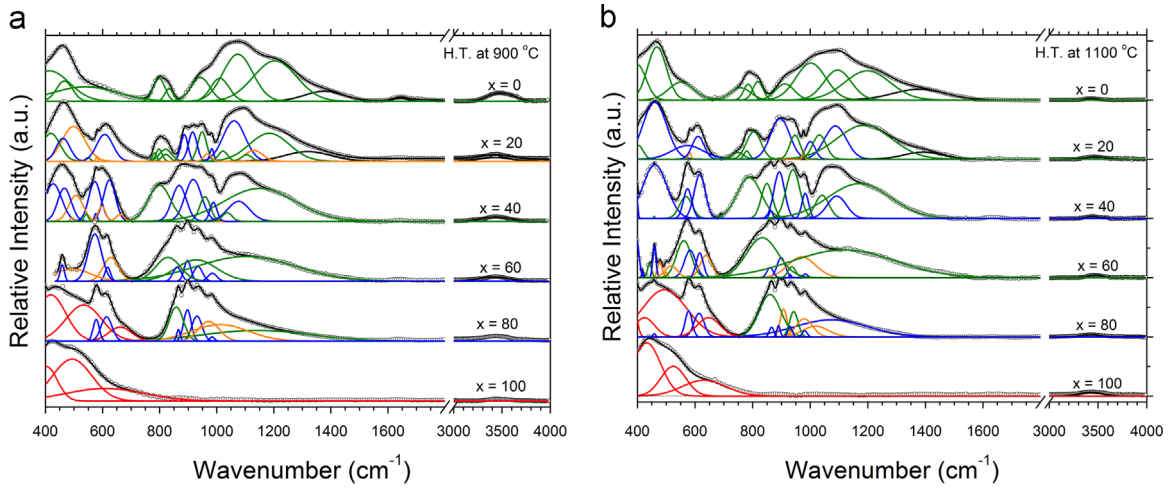

Fig. 2. FTIR spectra of $(100-x)SiO_2$:$xZnO$ powders containing 1.0 mol% of Er^{3+} annealed at (a) 900 °C, and (b) 1100 °C. (For interpretation of the references to color in this figure, the reader is referred to the web version of this article.)

Table 2
Vibrational band position for different samples annealed at 900 and 1100 °C [43,44].

X value		0		20		40		60		80		100		Assignments	Phase
	Tempe-rature (°C)	900	1100	900	1100	900	1100	900	1100	900	1100	900	1100		
Band position (cm^{-1})		413	400	418	403	-	-	-	-	-	-	-	-	Un-polymerized SiO_4	a-SiO_2
		-	-	-	-	428	400	-	418	-	-	-	-	v_4-SiO_4,[29]	Willemite
		466	466	-	-	-	458	-	441	-	-	-	-	Un-polymerized SiO_4	a-SiO_2
		-	-	-	-	-	-	-	-	418	424	404	432	ZnO,[43]	Zincite
		-	-	461	461	467	460	459	459	-	459	-	-	v_4-SiO_4,[26]	Willemite
		-	-	498	-	496	-	-	478	-	-	-	-	Si-O bond bending,[30] and/or Polymerized ZnO_4,[44]	unknown
		-	-	-	-	507	-	496	499	-	-	-	-		
		-	-	-	-	-	-	-	517	-	-	-	-		
		-	-	-	-	-	-	-	-	534	494	494	525	ZnO,[43]	Zincite
		542	551	550	-	542	569	-	561	-	-	-	-	SiO_2	a-SiO_2
		-	-	-	572	573	575	573	582	578	579	-	-	v_1-ZnO_4,[29, 30]	Willemite
		-	-	-	-	577	-	-	-	-	-	-	-	–	unknown
		-	-	580	580	598	-	-	-	-	-	-	-	–	
		-	-	607	613	625	617	617	617	615	613	-	-	v_1-ZnO_4,[29]	Zn_2SiO_4
		-	-	656	-	661	-	629	638	-	-	-	-	–	unknown
		-	-	-	-	-	-	-	-	661	648	609	630	ZnO	Zincite
		-	758	783	748	-	690	-	-	-	-	-	-	SiO_2	a-SiO_2
		799	785	799	779	800	788	-	-	-	-	-	-	SiO_2,[43]	a-SiO_2
		833	818	821	804	-	850	829	833	858	859	-	-	Si-O-Si symmetric stretching,[30]	a-SiO_2
		-	-	-	-	868	863	862	860	867	866	-	-	v_1-SiO_4,[1]	Willemite
		-	-	887	897	-	893	897	898	897	889	-	-	Si-O_4 bands,[30]	Willemite
		-	-	-	-	-	-	-	-	-	907	-	-	Si-O-Si	
		-	-	916	-	918	-	928	930	931	929	-	-	v_3-SiO_4,[29]	Willemite
		945	912	949	947	958	939	935	935	-	943	-	-	Un-polymerized SiO_4,[44]	a-SiO_2
		-	-	968	977	-	-	-	970	972	979	-	-	Un-polymerized SiO_4,[44]	unknown
		-	-	983	1000	989	984	985	983	983	981	-	-	Si-O_4 bands,[30]	Willemite
		1012	1003	1022	1032	1037	1041	-	-	1014	1018	-	-	Polymerized SiO_4,[31] Si-O-Si bands,[30]	a-SiO_2
		-	-	1060	1088	1076	1091	-	-	-	1074	-	-	v_3-Si-O-Si,[29]	Willemite
		1072	1094	1105	-	-	-	1103	1116	1140	-	-	-	Polymerized SiO_4,[31]	a-SiO_2
		-	-	1130	-	-	-	-	-		-	-	-	Polymerized SiO_4,[31]	unknown
		1205	1200	1184	1188	1151	1170	-	-	-	-	-	-	Polymerized SiO_4,[31]	a-SiO_2
		1379	1379	1319	1392	-	-	-	-	-	-	-	-	COO^- or CH_3,[29]	-
		1645	-	-	-	-	-	-	-	-	-	-	-	Si-OH,[29]	-
		3450	-	-	-	-	-	-	-	-	-	-	-	Si-OH,[29]	-

'v_4' is the asymmetric deformation vibrations, respectively, in good agreement with the present results (Table 2). The samples for $x=0$ annealed at 1100 °C ($100SiO_2$) have bands centered at 400, 466, 551, 758, 785, 818, 912, 1003, 1094, and 1200 cm^{-1} of Si–O–Si vibrations, while ZnO crystalline structure ($x=100$ at 1100 °C) possess bands at 432, 525 and 630 cm^{-1}. The main peaks in the spectra, localized around 1000 and 1200 cm^{-1}, are typical of silica-based glassy materials. According to Almeida et al. [31], the band localized at 1075 cm^{-1} is assigned to the asymmetric stretching of the transversal optical component, while the shoulder around 1185 cm^{-1} is attributed to the stretching of the longitudinal optical component of the Si–O–Si group, evidencing formation of the SiO_2 network. This shoulder at around 1185 cm^{-1} is more evident in systems with high porosity [32].

In this sense, this work shows that the relative absorption band around 1185 cm^{-1} decreases as a function of the ZnO content. This behavior is an indication that the heat treatment promotes densification of the materials, as observed from the band assigned to the OH groups (band centered at ~3450 cm^{-1}), whose intensity reduced as a function of the ZnO content (Fig. 2(a)).

The absorption peaks at 1645 cm^{-1} and 3450 cm^{-1} become less intense as the heating temperatures and ZnO content increase. Weak O–H stretching can be found in sample annealed at 900 °C due to water absorption from the surface or internal silanols and alcohol during the synthesis [29]. The heat treatment at 1100 °C

for $x=40$ and 60 almost eliminate the hydroxyl groups, as monitored by the intensity of the absorption at around 3450 cm^{-1}.

The band at 1379 cm^{-1} for $x=0$ and $x=20$ are due to COO^- or CH_3 groups from citric acid. Efficient elimination of these organic groups was observed, mainly at high ZnO concentration and annealing temperature, suggesting that Zn^{2+} ions act as catalyst.

The temperature and ZnO concentration are important to control the structural properties, with emphasis on the erbium ions distribution in the host, and the complete elimination of organic and/or hydroxyl groups. The homogeneous distribution of erbium ions is important to avoid cluster formation, which may give rise to non-radiative decay by the energy migration between rare earth ions and consequently leading to luminescence quenching. On the other hand, the hydroxyl and organic groups can promote non-radiative decay of the excited levels of Er^{3+} ions by multiphonon relaxation, which also can contribute to quench the luminescence reducing the emission quantum efficiency [9].

In fact, some structural parameters can play important role on the Er^{3+} ion emissions, as well its emission band broadening, transition probability, emission intensity, metastable level lifetime and radiative emission quantum efficiency, such as phonon energy, refractive index of the host, the concentration and dispersion of ions in the matrix, and the local structure (symmetry) around the rare-earth ions. The phonon energy is related to the non-radiative transition probability of the doped rare-earth ions. Furthermore, the refractive index has an influence on the emission cross-section of rare-earth ions. Wide infrared transmittance and good chemical stability are other characteristics that can take into account for the development of Er^{3+}-doped amplifiers based on glasses or glass-ceramics. Moreover, the modification of the rare-earth spectral properties by addition of zinc oxide within glasses can be promising to obtain a broad amplifier bandwidth with an intrinsically flat gain required in the development of optical transmission network. The presence of hydroxyl within the matrix has a great influence on quenching effects on the excited levels of Er^{3+} concerned with the radiative emission. A decrease in the hydroxyl concentration is necessary, and consequently, the damaging effect induced by migration to impurities like hydroxyl groups should be limited [33,34].

The mixture of crystalline and amorphous phases in our samples can be of great interest to increase the emission intensity and broadening around 1533 nm (0.809 eV) due to the transition between $^4I_{13/2}$ and $^4I_{15/2}$ levels of Er^{3+} ions.

The effect of SiO_2:ZnO relation and annealing temperature are also critical, as will be discussed bellow.

3.2. Optical studies

The photoluminescence (PL) emission spectra are shown in Fig. 3 for different compositions and heat-treated from 800 °C to 1100 °C under excitation at 980 nm. The Er^{3+} emission in the NIR region due to the $^4I_{13/2} \rightarrow {}^4I_{15/2}$ transition, collected from 0.886 eV

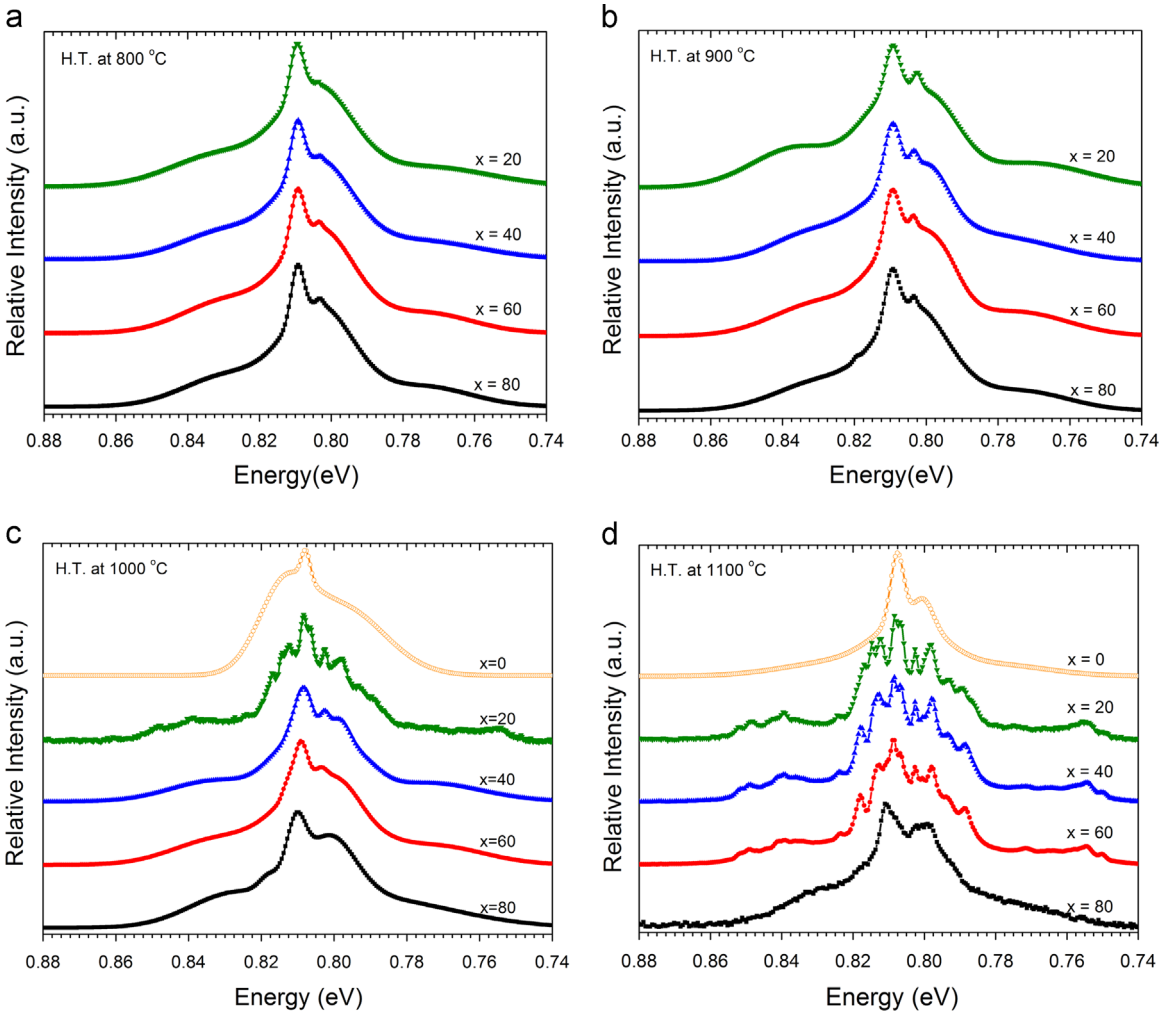

Fig. 3. Photoluminescence emission of $(100-x)SiO_2$:$xZnO$ powders containing 1.0 mol% of Er^{3+} annealed at (a) 800 °C, (b) 900 °C, (c) 1000 °C, and (d) 1100 °C excited at 980 nm.

(1400 nm) to 0.730 eV (1700 nm), shows a broad band centered on 0.809 eV (1533 nm), with no evidence of visible upconversion PL even at 250 mW pump powers. This infrared emission is affected by the host site of the rare earth ion, in which the influence of Stark effect on metastable level $^4I_{13/2}$ of Er^{3+} ions was observed.

Only samples containing both SiO_2 and ZnO annealed at 800 and 900 °C emit in the near infrared region, showing predominantly Er^{3+} ions in an amorphous phase. For heat treatment at 1000 °C, only sample with $x=20$ possess a better defined Stark effect similar to that measured for powders annealed at 1100 °C. Moreover, samples with $x=20$, 40 and 60 present a well defined Stark effect, suggesting the dispersion of Er^{3+} ions into Zn_2SiO_4 rhombohedral phase, which was characterized by XRD and FTIR analysis. These mixed composition present emission spectra with full width at half-medium (FWHM) between 40 and 48 nm, in contrast with $x=0$ sample (SiO_2) having FWHM of 25 nm. Zampedri et al. [35] have found a FWHM of about 51 nm in a 1.0 mol% Er^{3+} doped 80%SiO_2:20%TiO_2 thin films annealed at 900 °C. Gonçalves and co-workers [36] have measured a FWHM of 48 nm in a 0.3 mol% Er^{3+} doped 70%SiO_2:30%HfO_2 waveguides synthesized at 900 °C. Recently, we have reported a bandwidth value of 34 nm in 80%SiO_2:20%ZrO_2 films containing 0.3 mol% of Er^{3+} at 900 °C from the sol–gel process [37].

Fig. 4 shows the intensity emission of Er^{3+} in the studied system. As it can see, the higher emission occurs for the sample with $x=60$ annealed at 1100 °C. This emission enhancement is linked to the structure, mainly composed by the crystalline Willemite and small amount of amorphous SiO_2, resulting in a high dispersion of Er^{3+} ions in the matrix structure.

There are two non-equivalent crystallographic Zn sites in Zn_2SiO_4 rhombohedral structure with the distorted tetrahedral coordination of oxygen. The main difference is in the average dimensions of the two Zn tetrahedral ($<$Zn–O$>$ from 1.729 to 2.193 Å), and the silicon ions are also in tetrahedral coordination with oxygen ions ($<$Si–O$>$ from 1.582 to 1.670 Å), as described elsewhere [27,38,39]. Dacanin and co-workers [38] studied the incorporation of Eu^{3+} ions into Zn_2SiO_4 rhombohedral structure, in which Eu^{3+} ions may be placed at both Zn sites with negligible differences on the PL emission spectra [38]. Also, the structure of Zn_2SiO_4 rhombohedral is composed by an empty long hexagonal tube, and made up of six tetrahedral chains, as described in reference [27]. In our $x=20$, 40, and 60 samples annealed at 1100 °C we observe the same spectra, suggesting that Er^{3+} ions occupy both Zn sites of the Zn_2SiO_4 rhombohedral structure. We can also propose that part of the Er^{3+} ions can be located into the empty hexagonal tube, because the Er^{3+} ionic radius, 0.88 Å [40], is smaller than the diameter of that tube in the Zn_2SiO_4 structure.

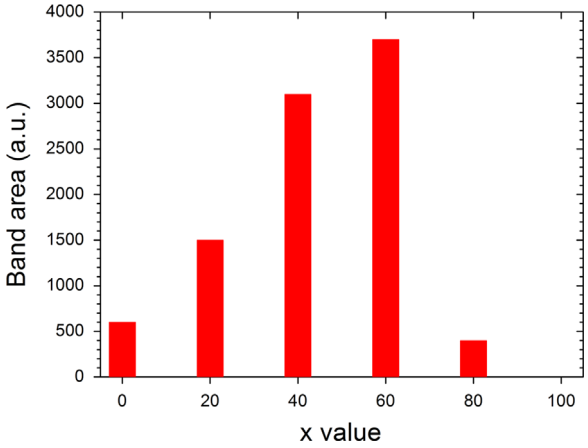

Fig. 4. Emission intensity (band area) for samples annealed at 1100 °C as a function of ZnO concentration (x value).

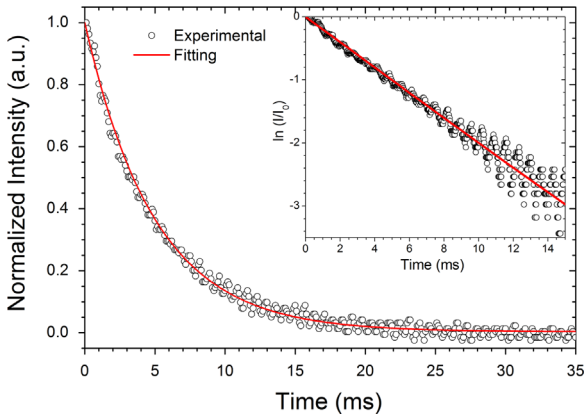

Fig. 5. Photoluminescence decay curve (experimental and fitting) from Er^{3+} doped sample containing $x=60$ annealed at 1100 °C excited at 980 nm.

Table 3
Experimental $^4I_{13/2}$ lifetime values (τ of Er^{3+} doped samples.

x Value	Temperature (°C)			
	800	900	1000	1100
20	–	–	–	4.4 ± 0.1 (42 nm)
40	–	–	–	4.6 ± 0.1 (45 nm)
60	4.7 ± 0.1 (40 nm)	4.7 ± 0.1 (43 nm)	4.9 ± 0.1 (43 nm)	5.0 ± 0.1 (45 nm)
80	–	–	–	4.5 ± 0.3 (48 nm)

In parentheses is the FWHM of the emission band at ~1533 nm (0.809 eV).

Fig. 5 depicts the PL decay curve for the $^4I_{13/2}$ level of Er^{3+} for $x=60$ (40SiO_2:60ZnO) sample heat-treated at 1100 °C. The best fit adjusted for the exponential curve was the first-order type (monoexponential), which is representative of all other samples. Table 3 lists the calculated lifetime values and uncertainties as a function of the temperature and x values. It was shown only the lifetime value of the samples presenting higher PL emissions. The samples with weak PL emission the decay curves could not be measured due to the sensitivity of detection system. Almost all lifetime uncertainties are 0.1 ms, except for $x=80$ sample heat-treated at 1100 °C is 0.3 ms because smaller PL emission intensity. The average lifetime values increase for higher temperatures, and a maximum value of 5.0 ± 0.1 ms was observed at 1100 °C for $x=60$. Comparing the τ values for all samples, note that $x=60$ possesses the highest value leading to a highest PL emission intensity.

The $^4I_{13/2}$ PL lifetimes are comparable to other silicate nanocomposites doped with much less Er^{3+} concentration [41], higher than in phosphate glass (4.0 ms) [42], but considerable longer than yttrium alumino based borate (0.64 ms) glassy powders [8]. Also, Zampedri et al. [35] measured a lifetime of 3.5 ms in a 1.0 mol% Er^{3+} doped 80%SiO_2:20%TiO_2 thin films. Gonçalves and co-workers observed a lifetime of 5.0 ms in a 0.3 mol% Er^{3+} doped 70%SiO_2:30%HfO_2 waveguides [36], and of 6.4 ms for 80%SiO_2:20%ZrO_2 films containing 0.3 mol% of Er^{3+}[37]. Besides, Mais et al. [16] have measured a lifetime of about 7.0 ms for Er amount of 2 at% in ZnO planar waveguide structure.

In general, the lifetime of $^4I_{13/2}$ level of Er^{3+} ions is strongly governed by radiative and non-radiative process. Our observations show the mono-exponential nature of the decay at 1.0 mol% of Er^{3+} ions with a lifetime of 5.0 ms. However, for the pure ZnO host doped with 1.0 mol% of Er^{3+} no emission at 1533 nm could be detected, probably due to Er^{3+} ions segregation that takes place at high temperatures.

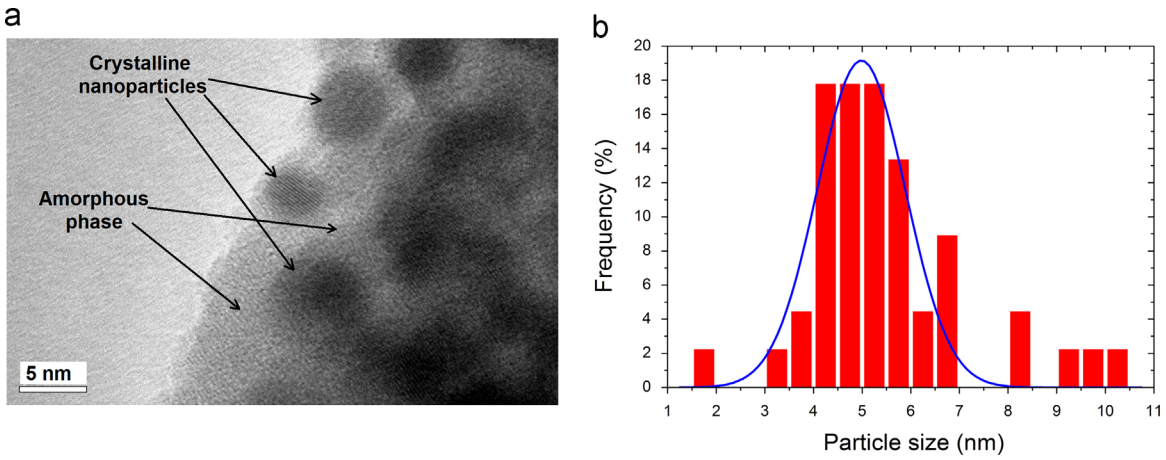

Fig. 6. (a) HRTEM image, and (b) histogram of the $x=60$ sample annealed at 1100 °C. Statistical histogram was obtained from the HRTEM images.

3.3. Morphological characteristics

Fig. 6(a) illustrates the HRTEM images of the sample with $x=60$ and heat-treated at 1100 °C. The presence of Zn_2SiO_4 rhombohedral spherical shape nanoparticles embedded into the amorphous phase can be noted for the compound. The densification process occurs together with the crystallization, where Zn_2SiO_4 nanocrystals with sizes around 5 nm are dispersed into the amorphous silica-based matrix. The determined interplanar distance is 2.32 ± 0.04 Å, which can be related to the (223−) plane for Zn_2SiO_4 rhombohedral crystalline phase (Willemite), as comparable with value (2.32) in the JCPDS card number 70-1235. Fig. 6 (b) corresponds to the statistical histogram of the size distribution of the Zn_2SiO_4 nanoparticles, which is narrow. These Zn_2SiO_4 nanosized crystalline structures could be also responsible for the PL emission enhancement of Er^{3+} ions, as observed previously for ZnO nanorods [17].

4. Conclusions

It was presented an easy and low cost synthesis route to prepare homogeneous SiO_2:ZnO gels and powders containing 1.0 mol% of Er^{3+} with no requirements of pH and atmosphere control. Samples with high erbium ions concentration (1.0 mol%) were prepared, and its structure and PL emission from $^4I_{13/2}$ to $^4I_{15/2}$ transition was evaluate as a function of relative ZnO concentration and annealing temperature. Only rhombohedral Willemite phase (Zn_2SiO_4) was crystallized in powders with $x=60$ from 900 °C to 1100 °C, and with $x=40$ for 1000 °C and 1100 °C, however the FTIR results reveal also a small amount of an amorphous phase in these samples. The $x=60$ sample annealed at 1100 °C presented higher PL emission in the infrared region with average lifetime of 5.0 ± 0.1 ms of the $^4/_{13/2}$ level, which can be related to Willemite phase. The Zn_2SiO_4 rhombohedral spherical shape nanoparticles of ~5 nm are embedded into the amorphous phase as observed by HRTEM results. The SiO_2:ZnO composite samples containing 1.0 mol% of Er^{3+} show higher FWHM values than SiO_2 ones ($x=0$). In the case of ZnO sample ($x=100$), no emission of Er^{3+} ions were observed for this high erbium concentration studied.

Conclusively, the rare earth doped zinc silicate ($40SiO_2$:60ZnO doped with 1.0 mol% of Er^{3+}) material has high potential for application as optical amplifiers in the near infrared region.

Acknowledgments

The financial support of FAPESP, CAPES, FUNAPE, and CNPq (Brazilian agencies) is gratefully acknowledged. The authors wish to thanks the Microscopy Laboratory (LabMic) of the Universidade Federal de Goiás (UFG) for HRTEM images.

References

[1] L.D. Carlos, R.A.S. Ferreira, V.D. Bermudez, S.J.L. Ribeiro, Adv. Mater. 21 (5) (2009) 509.
[2] S. Tanaka, Y. Ishikawa, N. Shibata, J. Ceram. Soc. Japan 115 (1341) (2007) 341.
[3] Z. Pan, S.H. Morgan, A. Ueda, R. Aga Jr, A. Steigerwald, A.B. Hmelo, R. Mu, J. Phys.: Cond. Matter 19 (26) (2007) 266216.
[4] L.J.Q. Maia, C.R. Ferrari, V.R. Mastelaro, A.C. Hernandes, A. Ibanez, Solid State Sci. 10 (12) (2008) 1835.
[5] M. Karbowiak, J. Cichos, C.J. Rudowicz, Phys. Chem. A 116 (43) (2012) 10574.
[6] Y.Y. Guo, M. Li, L.L. Hu, J.J. Zhang, J. Phys. Chem. A 116 (23) (2012) 5571.
[7] A. Florez, Y. Messaddeq, O.L. Malta, M.A. Aegerter, J. Alloy. Compd. 227 (1995) 135.
[8] L.J.Q. Maia, V.R. Mastelaro, A.C. Hernandes, J. Fick, A. Ibanez, Thin Solid Films 517 (24) (2009) 6584.
[9] R.K. Verma, K. Kumar, S.B. Rai, J. Lumin. 131 (5) (2011) 988.
[10] P.K. Sharma, R.K. Dutta, M. Kumar, P.K. Singh, A.C. Pandey, J. Lumin. 129 (6) (2009) 605.
[11] J. Iqbal, X. Liu, H. Zhu, Z.B. Wu, Y. Zhang, D. Yu, R. Yu, Acta Mater. 57 (16) (2009) 4790.
[12] D. Comedi, M. Tirado, C. Zapata, S.P. Heluani, M. Villafuerte, P.K. Mohseni, R.R. LaPierre, J. Alloy. Compd. 495 (2) (2010) 439.
[13] F. Xiao, R. Chen, Y.Q. Shen, B. Liu, G.G. Gurzadyan, Z.L. Dong, Q.Y. Zhang, H.D. Sun, J. Alloy. Compd. 509 (29) (2011) 7794.
[14] Z. Xu, Y. Wang, J. Alloy. Compd. 555 (2013) 268.
[15] M. Kohls, T. Schmidt, H. Katschorek, L. Spanhel, G. Muller, N. Mais, A. Wolf, A. Forchel, Adv. Mater. 11 (4) (1999) 288.
[16] N. Mais, J.P. Reithmaier, A. Forchel, M. Kohls, L. Spanhel, G. Muller, Appl. Phys. Lett. 75 (14) (1999) 2005.
[17] J.W. Lo, C.A. Lin, J.H. He, Curr. Nanosci. 7 (2) (2011) 282.
[18] S. Panigrahi, A. Bera, D. Basak, J. Colloid Interf. Sci. 353 (1) (2011) 30.
[19] K. Vanheusden, W.L. Warren, C.H. Seager, D.R. Tallant, J.A. Voigt, B.E. Gnade, J. Appl. Phys. 79 (10) (1996) 7983.
[20] D.C. Reynolds, D.C. Look, B. Jogai, J. Appl. Phys. 89 (11) (2001) 6189.
[21] J.Q. Hu, Y. Bando, Appl. Phys. Lett. 82 (9) (2003) 1401.
[22] S.A. Studenikin, M. Cocivera, J. Appl. Phys. 91 (8) (2002) 5060.
[23] A. Barker, S. Crowther, D. Rees, Sens. Actuators A: Phys. 58 (3) (1997) 229.
[24] J.G. Ma, Y.C. Liu, C.S. Xu, Y.X. Liu, C.L. Shao, H.Y. Xu, J.Y. Zhang, Y.M. Lu, D.Z. Shen, X.W. Fan, J. Appl. Phys. 97 (10) (2005) 103509.
[25] R. Anedda, C. Cannas, A. Musinu, G. Pinna, G. Piccaluga, M. Casu, J. Nanoparticle Res. 10 (1) (2008) 107.
[26] M. Takesue, H. Hayashi, R.L. Smith Jr, Prog. Cryst. Growth Charact. Mater. 55 (3–4) (2009) 98.
[27] R.M. Krsmanovic, Z. Antic, M. Mitric, M.D. Dramicanin, M.G. Brik, Appl. Phys. A: Mater. Sci. Process. 104 (1) (2011) 483.
[28] C.C. Baker, J. Heikenfeld, Z. Yu, A.J. Steckl, Appl. Phys. Lett. 84 (9) (2004) 1462.
[29] P. Sharma, H.S. Bhatti, J. Alloy. Compd. 473 (1–2) (2009) 483.
[30] Y. Wu, Y. Wang, D. He, M. Fu, Z. Chen, Y. Li, J. Lumin. 130 (10) (2010) 1768.

[31] R.M. Almeida, T.A. Guiton, C.G. Pantano, J. Non-Cryst. Solids 121 (1–3) (1990) 193.
[32] J.L. Ferrari, K.O. Lima, L.J.Q. Maia, S.J.L. Ribeiro, R.R. Goncalves, J. Am. Ceram. Soc. 94 (4) (2011) 1230.
[33] V. Nazabal, S. Todoroki, A. Nukui, T. Matsumoto, S. Suehara, T. Hondo, T. Araki, S. Inoue, C. Rivero, T. Cardinal, J. Non-Cryst. Solids 325 (1–3) (2003) 85.
[34] L. Zampedri, M. Mattarelli, M. Montagna, R.R. Gonçalves, Phys. Rev. B 75 (7) (2007) 073105.
[35] L. Zampedri, M. Ferrari, C. Armellini, F. Visintainer, C. Tosello, S. Ronchin, R. Rolli, M. Montagna, A. Chiasera, S. Pelli, G.C. Righini, A. Monteil, C. Duverger, R.R. Gonçalves, J. Sol–Gel Sci. Technol. 26 (1–3) (2003) 1033.
[36] R.R. Goncalves, G. Carturan, L. Zampedri, M. Ferrari, M. Montagna, A. Chiasera, G.C. Righini, S. Pelli, S.J.L. Ribeiro, Y. Messaddeq, Appl. Phys. Lett. 81 (1) (2002) 28.
[37] R.R. Goncalves, J.J. Guimarães, J.L. Ferrari, L.J.Q. Maia, S.J.L. Ribeiro, J. Non-Cryst. Solids 354 (42–44) (2008) 4846.
[38] L. Dacanin, S.R. Lukic, D.M. Petrovic, M. Nikolic, M.D. Dramicanin, Physica B 406 (11) (2011) 2319.
[39] Y.I. Kim, W. Bin Im, K.S. Ryu, K.B. Kim, Y.H. Lee, J.S. Lee, Nucl. Instrum. Meth. Phys. Res. B 268 (3–4) (2010) 346.
[40] F. Rocca, C. Armellini, M. Ferrari, G. Dalba, N. Diab, A. Kuzmin, F. Monti, J. Sol–Gel Sci. Technol. 26 (1–3) (2003) 267.
[41] J.L. Ferrari, K.O. Lima, L.J.Q. Maia, R.R. Goncalves, Thin Solid Films 519 (4) (2010) 1319.
[42] Y.C. Yan, A.J. Faber, H. de Waal, P.G. Kik, A. Polman, Appl. Phys. Lett. 71 (20) (1997) 2922.
[43] A.M. Pires, M.R. Davolos, Chem. Mater. 13 (1) (2001) 21.
[44] B.A. Sava, A. Diaconu, M. Elisa, C.E.A. Grigorescu, I.C. Vasiliu, A. Manea, Superlatt. Microstruct. 42 (1–6) (2007) 314.